Research Square

Preprints are preliminary reports that have not undergone peer review.
They should not be considered conclusive, used to inform clinical practice,
or referenced by the media as validated information.

Zn-modified Li3Mg2SbO6 microwave dielectric ceramics with high quality factor

Hongyang Zhang
University of Electronic Science and Technology of China
Cheng Liu (c_liu@uestc.edu.cn)
University of Electronic Science and Technology of China https://orcid.org/0000-0002-0845-5777
Liang Shi
University of Electronic Science and Technology of China
Wenwen Wang
University of Electronic Science and Technology of China
Wenhao Xu
University of Electronic Science and Technology of China
Gang Wang
University of Electronic Science and Technology of China
Xing Zhang
University of Electronic Science and Technology of China
Rui Zeng
University of Electronic Science and Technology of China
Huaiwu Zhang
University of Electronic Science and Technology of China

Research Article

Keywords: Microwave dielectric properties, Li3Mg2SbO6, High quality factor, Ceramics

Posted Date: July 20th, 2020

DOI: https://doi.org/10.21203/rs.3.rs-44208/v1

License: This work is licensed under a Creative Commons Attribution 4.0 International License.
Read Full License

Version of Record: A version of this preprint was published at Journal of Materials Science: Materials in Electronics on February 13th, 2021. See the published version at https://doi.org/10.1007/s10854-021-05345-3.

Abstract

Well-densified $Li_3(Mg_{1-x}Zn_x)_2SbO_6$ ($0.00 \leq x \leq 0.08$) microwave dielectric ceramics were synthesized via a two-stage sintering process. The effects of Zn^{2+} substitution on the microstructure and microwave dielectric properties were investigated. All samples were identified as pure phase via the XRD detection. Remarkable microwave dielectric properties with a near-zero τ_f value were obtained in the $Li_3(Mg_{1-x}Zn_x)_2SbO_6$ ($x = 0.04$) sample sintered at 1325 ℃ for 5 h: $\varepsilon_r = 7.8$, $Q \times f = 97{,}719$ GHz (13.4 GHz), τ_f =-6 ppm/℃. The high $Q \times f$ value was suggested to relate with the dense morphology and grain size effect. All experimental results indicate that the $Li_3(Mg_{1-x}Zn_x)_2SbO_6$ ceramics are promising for 5G communication applications.

1. Introduction

With the rapid development of wireless communication, high performanced microwave dielectric ceramics are widely applied to various components, such as antennas, resonators, and substrates, etc [1]. Microwave dielectric ceramics with low dielectric permittivity (ε_r), low loss (high $Q \times f$ value), and good thermal stability (near-zero τ_f value) are expected to play an important role in 5G communication devices due to their potentials in reducing the signal delay, enhancing the frequency selectivity, and broadening the working temperature range. Therefore, it is of great importance to explore new advanced microwave dielectrics and push the performance limits in new era [2, 3].

In recent years, $Li_3Mg_2NbO_6$-based ceramics with orthorhombic structure have attracted much attention due to its excellent microwave dielectric properties [4]. It is reported that partial Mg^{2+} ion-substitution could improve the microwave dielectric properties of $Li_3Mg_2NbO_6$-based ceramics [5–12]. West et al. reported that the $Li_3Mg_2SbO_6$ ceramics possessed the same structure with that of the $Li_3Mg_2NbO_6$ ceramics [13]. However, few works focused on the $Li_3Mg_2SbO_6$ systems due to its easy cracking characteristics during the sintering process, which were attributed to the reaction with individual oxide components. In addition, lower $Q \times f$ values caused by the secondary phase SbO_x also limited its practical application in microwave devices [14]. Pei et al. firstly reported synthesis of pure $Li_3Mg_2SbO_6$ ceramics without dehiscence using a two-stage process. Excellent microwave dielectric properties were obtained at the sintering temperature of 1300 ℃: $\varepsilon_r = 10.5$, $Q \times f = 84{,}600$ GHz and τ_f =-9 ppm/℃ [15]. The higher $Q \times f$ values make it potential for high frequency applications. However, more efforts are still requested to push the τ_f value towards zero.

In the present work, we modified $Li_3Mg_2SbO_6$ ceramics with Zn^{2+} substitution due to the close ion radii for Zn^{2+} (0.74 Å) and Mg^{2+} (0.72 Å) [16, 17], aiming at improving the sintering behavior and microwave dielectric performance of the $Li_3Mg_2SbO_6$ system to accommodate higher frequency applications. The microstructure and microwave dielectric properties of the $Li_3(Mg_{1-x}Zn_x)_2SbO_6$ ($0.00 \leq x \leq 0.08$) ceramics were investigated.

2. Experiment Procedure

High purity oxides and carbonate compounds MgO, ZnO, Sb_2O_3, and Li_2CO_3 (all purity > 99%) were used to synthesize the $Li_3(Mg_{1-x}Zn_x)_2SbO_6$ ($0.00 \leq x \leq 0.08$) ceramics by a two-stage sintering process. The precursors were weighed according to the stoichiometric formula of Li_3SbO_4, and milled with zirconia balls in distilled water for 8 h. Dried and sieved powders were then calcined at 900 ℃ for 4 h to form Li_3SbO_4 phase. Subsequently, MgO, ZnO, and Li_3SbO_4 precursors were weighed according to the formula of $Li_3(Mg_{1-x}Zn_x)_2SbO_6$ (x = 0.00, 0.02, 0.04, 0.06, 0.08) and then ball-milled for 8 h. After drying and sifting, the powders were granulated with 8 wt.% of Polyvinyl Acetate (PVA) binder and then compacted into cylinders with a diameter of 12 mm and a height of 6 mm under 100 MPa. The green pellets were sintered at a temperature range of 1275 ℃-1375 ℃ for 5 h in air with a heating rate of 2 ^{o}C/min.

The bulk density values were measured via the Archimedes method. The phase structure of the as-sintered ceramics was identified by an X-ray diffractometer (XRD, Miniflex 600, Japan) with a scanning rate of 5 ^{o}/min in the range of 10 °≤2θ ≤ 80 °. The surface morphology of the as-sintered samples was analyzed by a scanning electron microscope (SEM, JSM-6490, Japan). The microwave dielectric properties (ε_r, Q × f) were measured by the Hakki-Coleman dielectric resonator method using a cavity and a vector network analyzer (Agilent N5230A, USA). The temperature coefficient of resonant frequency (τ_f) was measured in the temperature range from 25 ℃ to 85 ℃ and was calculated by the following formula:

$$\tau_f = \frac{f_{85} - f_{25}}{f_{25}(85-25)} \times 10^{6} (ppm/℃) \qquad (1)$$

where f_{85} and f_{25} were the TE_{011} resonant frequencies at 85 ℃ and 25 ℃, respectively.

3. Results And Discussions

Figure 1 exhibits the XRD patterns of the $Li_3(Mg_{1-x}Zn_x)_2SbO_6$ ($0.00 \leq x \leq 0.08$) ceramics sintered at 1325 ℃ for 5 h. All the observed reflection peaks are indexed in terms of the $Li_3Mg_2SbO_6$ phase (JCPDS-PDF No. 36-1019) with the Fddd space group. No secondary phase diffraction peaks can be detected, indicating that a complete solid solution is formed in all compositions. Figure 1(b) shows that the (1 1 1) diffraction peak shifts towards lower angles with x increasing from 0.00 to 0.08. Such variation indicates that larger Zn^{2+} (ion radius = 0.74 Å) successfully substitute for Mg^{2+} (ion radius = 0.72 Å) sites [16, 17].

Figure 2 illustrates the SEM photos of the $Li_3(Mg_{1-x}Zn_x)_2SbO_6$ ($0.00 \leq x \leq 0.08$) ceramics sintered at 1325 ℃ for 5 h. As shown in Fig. 2(a)-(c), the samples presented homogeneous morphology with few pores detected and the average grain size rises slightly with x increasing from 0.00 to 0.04. However,

further increasing of the x value contributes nothing to the grain distribution but abnormal grain size distribution, as shown in Fig. 2(d-e). A case study of the sample with $x = 0.04$ sintered at 1350 °C manifests the abnormal morphology, as Fig. 2(f-g) shows. Therefore, a small amount of Zn^{2+} substitution for Mg^{2+} plays an important role in promoting the grain growth and morphology optimization. But excessive Zn^{2+} substitution inhibits the grain growth and deteriorate the homogeneous distribution of grains, which will deteriorate the dielectric properties. Linear intercept method is adopted to calculate the average grain size [18, 19]:

$$D = \frac{3L}{2MN} \tag{2}$$

where M, L, and N represent the actual magnification, the length of the test line, and the number of intersections, respectively. The calculated average grain size for the optimal densified sample is about 10.7 μm, which is obtained at the sintering temperature of 1325 ℃ and $x = 0.04$, as shown in Fig. 2(k).

Figure 3 presents the variation of the bulk density and permittivity of the $Li_3(Mg_{1-x}Zn_x)_2SbO_6$ ($0.00 \leq x \leq 0.08$) ceramics sintered at different temperatures. The density curves of different samples behave similar variation tendency, as shown in Fig. 3(a). Specifically, each density curve increases initially and reaches to a maximum value at 1325 ^{o}C~1350 ^{o}C, then decreases with the sintering temperature. In addition, the density values for different sample increase with x and reaches to a maximum at $x = 0.02$. The increase of the bulk density is mainly attributed to the elimination of pores and grain growth. However, abnormal grain size distribution induced by further Zn^{2+} substitution reduces the density, which matches well with the SEM results. The highest density value of 3.43 g/cm^3 was obtained in the sample of $x = 0.02$ at the sintering temperature of 1325 °C. Figure 3(b) shows the variation of the permittivity of the $Li_3(Mg_{1-x}Zn_x)_2SbO_6$ ($0.00 \leq x \leq 0.08$) ceramics sintered at different temperatures, which presents a similar tendency with the bulk density. In general, the dielectric permittivity is relevant to the porosity, phase constitution, and ionic polarizability [20, 21]. To eliminate the contribution of the porosity to the relative permittivity, the dielectric constant is corrected using the Eq. (3) [22]:

$$\frac{\varepsilon_{rm} - \varepsilon_2}{3\varepsilon_{rm}} = \frac{(1-p)(\varepsilon_{corr} - \varepsilon_2)}{\varepsilon_{corr} + 2\varepsilon_{rm}} \tag{3}$$

where p is the porosity fraction; ε_{rm}, ε_2, and ε_{corr} are the air, measured, and porosity corrected dielectric constants, respectively. The molecule polarizabilities are calculated according to Shannon by the ion polarizabilities, as described in Eq. (4) [21]:

$$\alpha_{theo}=3\alpha(Li^{+})+2(1-x)\alpha(Mg^{2+})+2x\,\alpha(Zn^{2+})+\alpha(Sb^{5+})+6\alpha(O^{2+}) \quad (4)$$

where $\alpha(Sb^{5+})$, $\alpha(Zn^{2+})$, $\alpha(Mg^{2+})$, $\alpha(O^{2-})$, and $\alpha(Li^{+})$ represent corresponding ion polarizability reported by Shannon [23]. The observed dielectric polarizabilities (α_{obs}) are obtained by the Clausius-Mossotti equation derived from Eq. (5) [24]:

$$\alpha_{obs} = \frac{1}{b} V_m \frac{\varepsilon_r - 1}{\varepsilon_r + 2} \quad (5)$$

where V_m and b indicate the molar volume and constant value ($4\pi/3$), respectively. The calculated results of τ_{corr}, α_{theo}, and α_{obs} values of the $Li_3(Mg_{1-x}Zn_x)_2SbO_6$ ceramics sintered at 1325 °C are listed in Table 1. It is observed that the α_{obs} and α_{theo} values present different variation trends, while the ε_r and τ_{corr} values exhibit similar tendency. As no secondary phases are detected via the XRD, the permittivity of the $Li_3(Mg_{1-x}Zn_x)_2SbO_6$ ceramics is mainly determined by the compactness. It is well known that higher density means lower porosity, which usually contributes to higher permittivity.

Figure 4 shows the Q × f values of the $Li_3(Mg_{1-x}Zn_x)_2SbO_6$ ($0.00 \le x \le 0.08$) ceramics sintered at different temperatures. The Q × f curves for different specimens present similar variation trends, increasing firstly and reaching to maximum values then declining with the sintering temperature. The maximum Q × f value of 97,719 GHz is obtained in the sample of $x = 0.04$ sintered at 1325 ℃, which is enhanced significantly compared with that of the previous study on $Li_3Mg_2SbO_6$ [15]. In general, the dielectric loss of the microwave ceramics is dominated by two primary factors: intrinsic structural characteristics such as packing fraction; and extrinsic factors such as the density, grain size, porosity, grain boundaries, and secondary phases [25–27]. As $Li_3(Mg_{1-x}Zn_x)_2SbO_6$ pure phase is detected, the Q × f values are mainly determined by the rest of the extrinsic factors except the secondary phase contribution. It is noticed that the maximum Q × f values for all samples except $Li_3Mg_2SbO_6$ are obtained at the sintering temperature of 1325 °C, slightly lower than their optimal densification temperature. The increment of the Q × f values can be attributed to the densification and grain growth with the sintering temperature, which eliminates some pores and defects, as shown in Fig. 2(a)-(e) and Fig. 3 [28, 29]. However, fuzzy grain boundaries emerge with further increasing of the sintering temperature to above 1325 ℃, which could deteriorate dielectric loss, as manifested in Fig. 2(f-g). Therefore, the comprehensive impacts on the Q × f value are related with the grain size, grain boundaries, and porosity [10].

Figure 5 exhibits the τ_f values of the $Li_3(Mg_{1-x}Zn_x)_2SbO_6$ ($0.00 \le x \le 0.08$) ceramics sintered at 1325 °C for 5 h. It is observed that the τ_f value ranges from − 12 to -1 ppm/°C in the range of $0.00 \le x \le 0.08$,

presenting an enhanced tendency with x. The introduction of Zn^{2+} into the $Li_3Mg_2SbO_6$ matrix for substituting Mg^{2+} could tune the τ_f value towards zero, implying that Zn^{2+} can effectively stabilize the crystal structure. Therefore, the substitution of Zn^{2+} for Mg^{2+} is considered as an effective solution to adjust the τ_f and improve the Q × f values of the $Li_3Mg_2SbO_6$ based systems, which is promising for 5G communication technology.

4. Conclusions

In this study, we synthesized $Li_3(Mg_{1-x}Zn_x)_2SbO_6$ ($0.00 \leq x \leq 0.08$) microwave dielectric ceramics via a two-stage sintering process and investigated the effects of Zn^{2+} substitution on the microstructure and microwave dielectric properties. Well-densified samples were identified as pure phase via the XRD detection. Remarkable microwave dielectric properties with a near-zero τ_f value were obtained in the $Li_3(Mg_{1-x}Zn_x)_2SbO_6$ (x = 0.04) sample sintered at 1325 ℃ for 5 h: ε_r = 7.8, Q × f = 97,719 GHz (13.4 GHz), τ_f =-6 ppm/℃. The high Q × f and near-zero τ_f values suggested that the substitution of Zn^{2+} for Mg^{2+} is an effective solution to tune the $Li_3Mg_2SbO_6$ based systems for 5G applications.

Declarations

Acknowledgments

This work was supported by Sichuan Science and Technology Program (No. 2020YFG0108), the National Natural Science Foundation of China (Grant No. 51672036), the National Key Scientific Instrument and Equipment Development Project (No.51827802), the Major Science and Technology Specific Projects of Sichuan Province (No. 2019ZDZX0026), and the Fundamental Research Funds for the Central Universities (Grant No. ZYGX2019J021).

References

1. Zhou D, Pang L-X, Wang D-W, Li C, Jin B-B, Reaney IM (2017) High permittivity and low loss microwave dielectrics suitable for 5G resonators and low temperature co-fired ceramic architecture. J Mater Chem C 5[38]:10094–10098
2. Nedelcu L, Toacsan MI, Banciu MG, Ioachim A, Microwave properties of $Ba(Zn_{1/3}Ta_{2/3})O_3$ dielectric resonators, J. Alloys Compd. 509[2] (2011) 477–481
3. Chen YB, New dielectric material system of $Nd(Mg_{1/2}Ti_{1/2})O_3$–$CaTiO_3$ with ZnO addition at microwave frequencies, J. Alloys Compd. 478[1–2] (2009) 781–784
4. Yuan L, Bian J (2009) Microwave dielectric properties of the lithium containing compounds with rock salt structure. Ferroelectrics 387(1):123–129
5. Zhang P, Wu S, Xiao M (2018) Effect of Sb^{5+} ion substitution for Nb^{5+} on crystal structure and microwave dielectric properties for $Li_3Mg_2NbO_6$ ceramics. J Alloys Compd 766:498–505

6. Wang G, Zhang D, Gan G, Yang Y, Rao Y, Xu F, Huang X, Liao Y, Li J, Liu C (2019) Synthesis, crystal structure and low loss of $Li_3Mg_2NbO_6$ ceramics by reaction sintering process. Ceram Int 45[16]:19766–19770
7. Zhang T, Zuo R, Effect of $Li_2O–V_2O_5$ addition on the sintering behavior and microwave dielectric properties of $Li_3(Mg_{1-x}Zn_x)_2NbO_6$ ceramics, Ceram. Int. 40[10] (2014) 15677–15684
8. Zhang P, Sun K, Xiao M, Zheng Z (2019) Crystal structure, densification, and microwave dielectric properties of $Li_3Mg_2(Nb_{1-x}Mo_x)O_{6+x/2}$ ($0 \le x \le 0.08$) ceramics. J Am Ceram Soc 102[7]:4127–4135
9. Zhang P, Sun K, Liu L, Xiao M (2018) A novel low loss and low temperature sintering $Li_3(Mg_{1-x}Ca_x)_2NbO_6$ microwave dielectric ceramics by doping LiF additives. J Alloys Compd 765:1209–1217
10. Zhang P, Liu L, Xiao M, Zhao Y, A novel temperature stable and high Q microwave dielectric ceramic in $Li_3(Mg_{1-x}Mn_x)_2NbO_6$ system, J. Mater. Sci.-Mater. Electron. 28[16] (2017) 12220–12225
11. Xing CF, Bi JX, Wu HT (2017) Effect of Co-substitution on microwave dielectric properties of $Li_3(Mg_{1-x}Co_x)_2NbO_6$ ($0.00 \le x \le 0.10$) ceramics. J Alloys Compd 719:58–62
12. Wang G, Zhang D, Xu F, Huang X, Yang Y, Gan G, Lai Y, Rao Y, Liu C, Li J, Jin L, Zhang H, Correlation between crystal structure and modified microwave dielectric characteristics of Cu^{2+} substituted $Li_3Mg_2NbO_6$ ceramics, Ceram. Int. 45[8] (2019) 10170–10175
13. Castellanos M, Gard JA, West AR (1982) Crystal data for a new family of phases, $Li_3Mg_2XO_6$:X = Nb, Ta, Sb. J Appl Crystallogr 15[1]:116–119
14. Yao G-g, Pei C, Gong Y, Ren Z, Liu P, Microwave dielectric properties of temperature stable $(1-x)Li_3Mg_2SbO_6–xBa_3(VO_4)_2$ composite ceramics, J. Mater. Sci.-Mater. Electron. 29[12] (2018) 9979–9983
15. Pei C, Hou C, Li Y, Yao G, Ren Z, Liu P, Zhang H (2019) A low εr and temperature-stable $Li_3Mg_2SbO_6$ microwave dielectric ceramics. J Alloys Compd 792:46–49
16. Zhao Y, Zhang P (2016) Microstructure and microwave dielectric properties of low loss materials $Li_3(Mg_{0.95}A_{0.05})_2NbO_6$ (A = Ca^{2+}, Ni^{2+}, Zn^{2+}, Mn^{2+}) with rock-salt structure. J Alloys Compd 658:744–748
17. Huang CL, Liu SS, Low-Loss Microwave Dielectrics in the $(Mg_{1-x}Zn_x)_2TiO_4$ Ceramics, J. Am. Ceram. Soc. 91[10] (2008) 3428–3430
18. Wang G, Zhang HW, Huang X, Xu F, Gan GW, Yang Y, Wen DD, Li J, Liu C, Jin LC (2018) Correlations between the structural characteristics and enhancedmicrowave dielectric properties of V-modified $Li_3Mg_2NbO_6$ ceramics. Ceram Int 44:19295–19300
19. Zheng HR, Yu SH, Li LX, Lyu XS, Sun Z, Chen SL (2017) Crystal structure, mixture behavior, and microwave dielectric properties of novel temperature stable $(1-x)MgMoO_4$-$xTiO_2$ composite ceramics. J Eur Ceram Soc 37:4661–4665

20. Zhang P, Xie H, Zhao Y, Zhao X, Xiao M (2017) Low temperature sintering and microwave dielectric properties of $Li_3Mg_2NbO_6$ ceramics doped with $Li_2O–B_2O_3–SiO_2$ glass. J Alloys Compd 690:688–691
21. Ping Z, Zhao Y, Li L (2015) The correlations among bond ionicity, lattice energy and microwave dielectric properties of $(Nd_{1-x}La_x)NbO_4$ ceramics. Phys Chem Chem Phys 17:16692–16698
22. Sebastian MT, Ubic R, Jantunen H (2015) Low-loss dielectric ceramic materials and their properties. Int Mater Rev 60:392–412
23. Shannon RD (1993) Dielectric polarizabilities of ions in oxides and fluorides. J Appl Phys 73[1]:348–366
24. Shannon RD, Rossman GR, Dielectric constants of silicate garnets and the oxide additivity rule, Am. Mineral. 77[1–2] (1992) 94–100
25. Penn SJ, Alford NM, Templeton A, Wang X, Schrapel K, Effect of Porosity and Grain Size on the Microwave Dielectric Properties of Sintered Alumina, J. Am. Ceram. Soc. 80[7] (2005) 1885–1888
26. Kume S, Yasuoka M, Omura N, Watari K, Effect of zirconia addition on dielectric loss and microstructure of aluminum nitride ceramics, Ceram. Int. 33[2] 269–272
27. Iddles DM, Bell AJ, Moulson AJ (1992) Relationships between dopants, microstructure and the microwave dielectric properties of ZrO_2-TiO_2-SnO_2 ceramics. J Mater Sci 27[23]:6303–6310
28. Wang G, Zhang H, Liu C, Su H, Li J, Huang X, Gan G, Xu F (2018) Low temperature sintering and microwave dielectric properties of novel temperature stable $Li_3Mg_2NbO_6$-0.1TiO_2 ceramics. Mater Lett 217:48–51
29. Huang CL, Yang WR, Yu PC (2014) High-Q microwave dielectrics in low-temperature sintered $(Zn_{1-x}Ni_x)_3Nb_2O_8$ ceramics. J Eur Ceram Soc 34[2]:277–284

Tables

Table Caption

Table 1. Theoretical dielectric polarizability (α_{theo}), observed dielectric polarizability (α_{obs}), dielectric constant (ε_r), quality factor ($Q \times f$), and temperature coefficient of resonant frequency (τ_f) of the $Li_3(Mg_{1-x}Zn_x)_2SbO_6$ ($0.00 \leq x \leq 0.08$) ceramics sintered at 1325 °C.

$Li_3(Mg_{1-x}Zn_x)_2SbO_6$	α_{theo}	α_{obs}	ε_r	ε_{corr}	$Q \times f$ (10^4 GHz)	τ_f (ppm/°C)
x = 0.00	22.57	19.13	8.13	10.87	6.87	-12
x = 0.02	22.60	19.48	8.47	11.06	8.10	-14
x = 0.04	22.63	19.35	8.25	10.94	9.77	-7
x = 0.06	22.66	18.34	7.71	10.45	5.31	-4
x = 0.08	22.69	18.39	7.19	9.95	5.18	-1

Figures

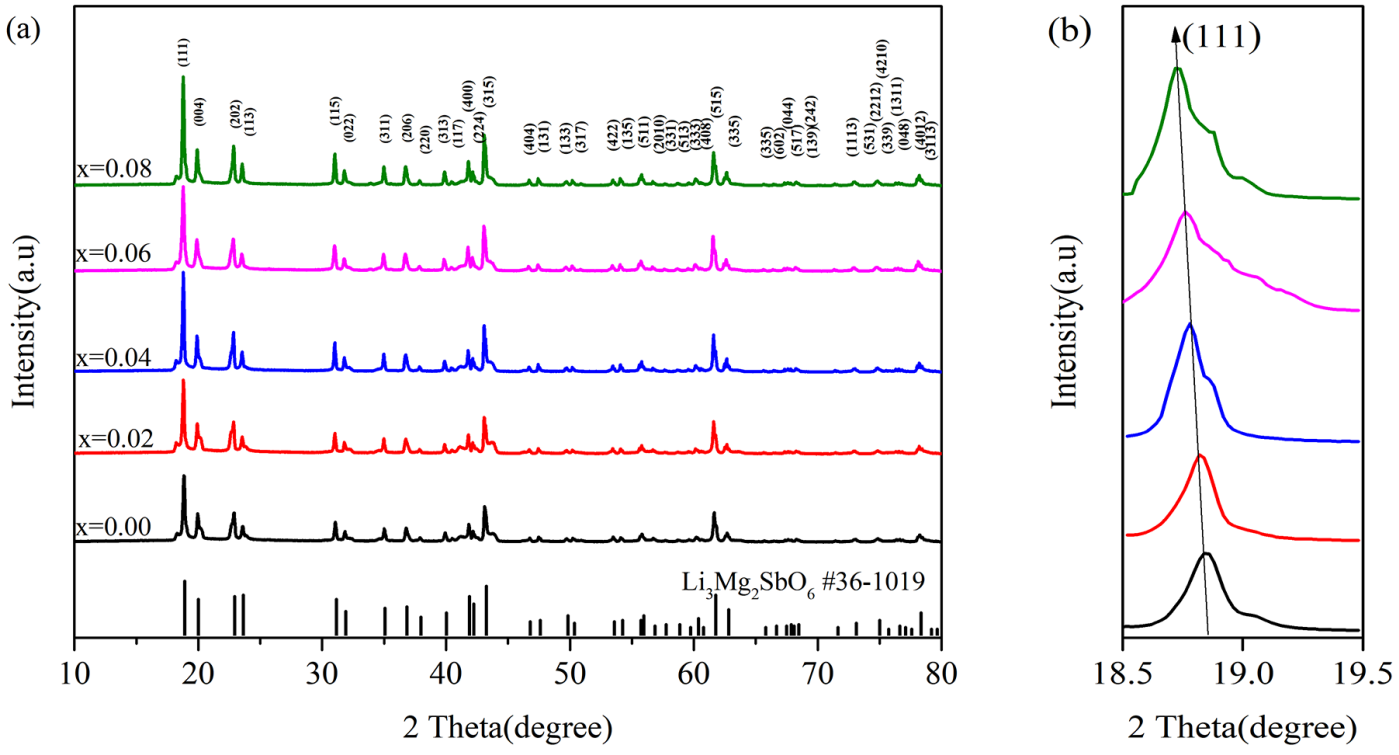

Figure 1

XRD diffraction patterns of the Li3(Mg1-xZnx)2SbO6 (0.00≤x≤0.08) ceramics sintered at 1325°C (a); and enlarged (1 1 1) diffraction peaks (b).

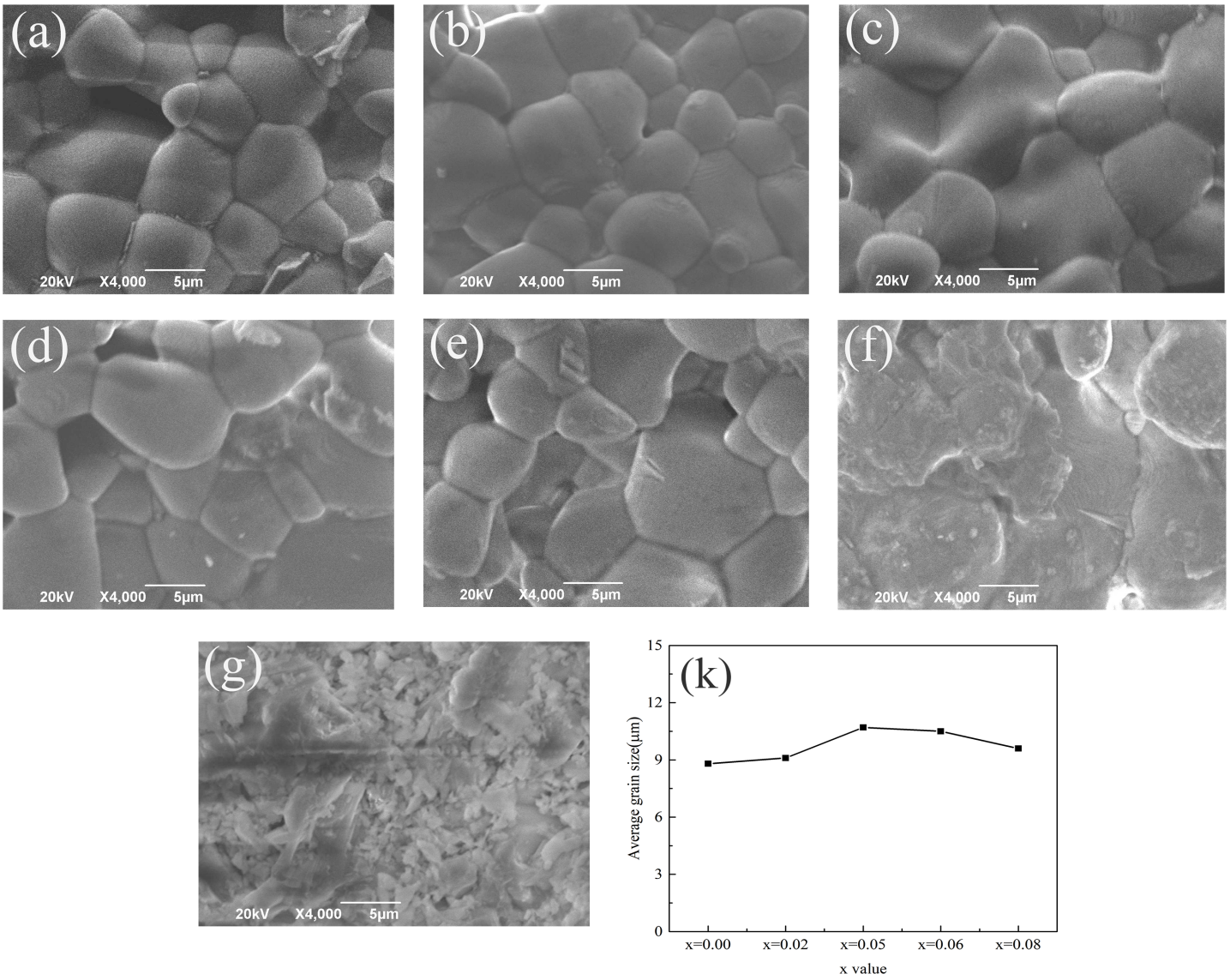

Figure 2

SEM photos of the Li3(Mg1-xZnx)2SbO6 (0.00≤x≤0.08) ceramics sintered at different temperature: (a) x=0.00, 1325 °C; (b) x=0.02, 1325 °C; (c) x=0.04, 1325 °C; (d) x=0.06, 1325 °C; (e) x=0.08, 1325 °C; (f) x=0.04, 1350 °C; (g) x=0.04, 1375 °C; (k) variation of the average grain size.

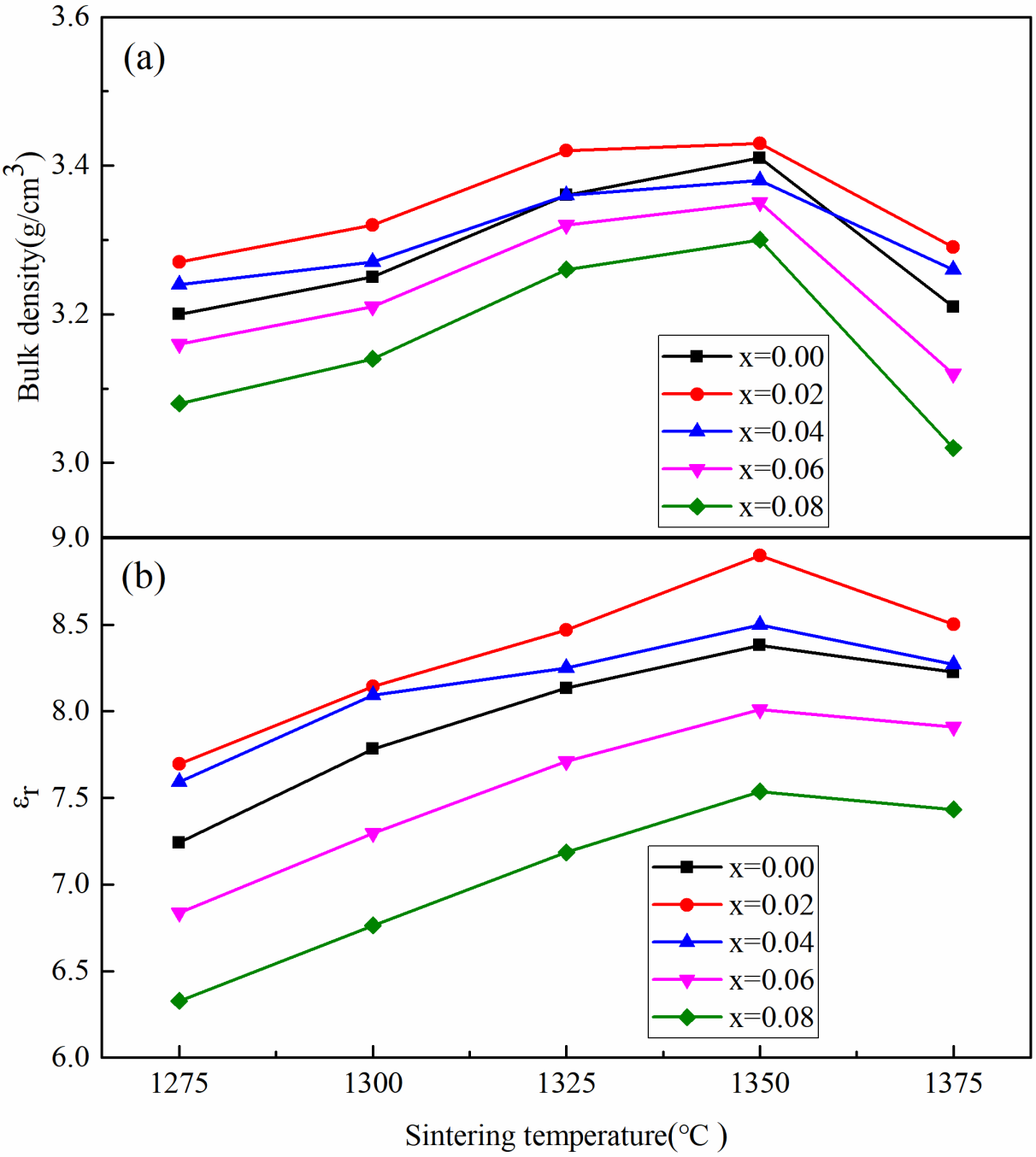

Figure 3

Bulk density (a) and permittivity (b) of the Li3(Mg1-xZnx)2SbO6 (0.00≤x≤0.08) ceramics sintered at various temperature.

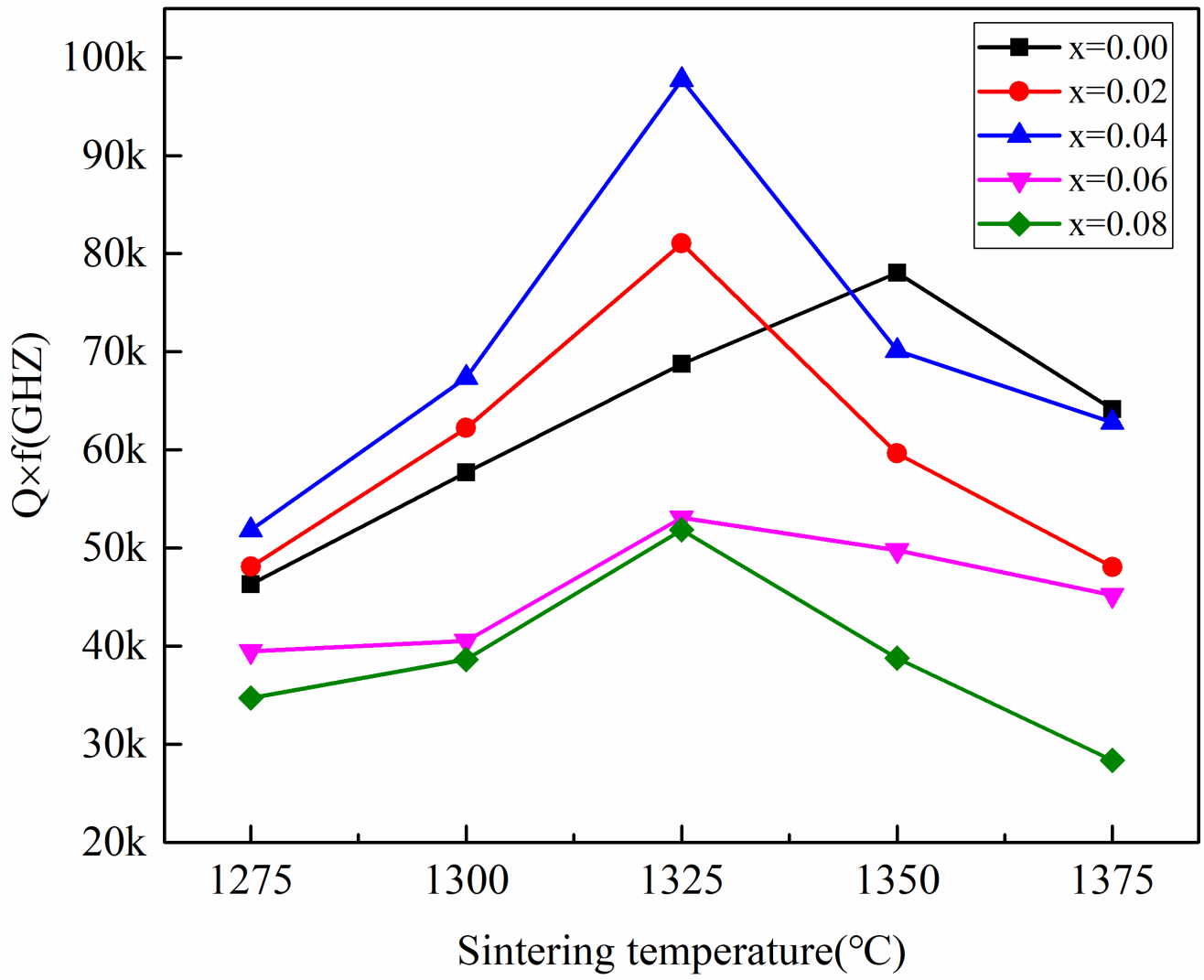

Figure 4

Q×f values of the Li3(Mg1-xZnx)2SbO6 (0.00≤x≤0.08) ceramics sintered at various temperatures.

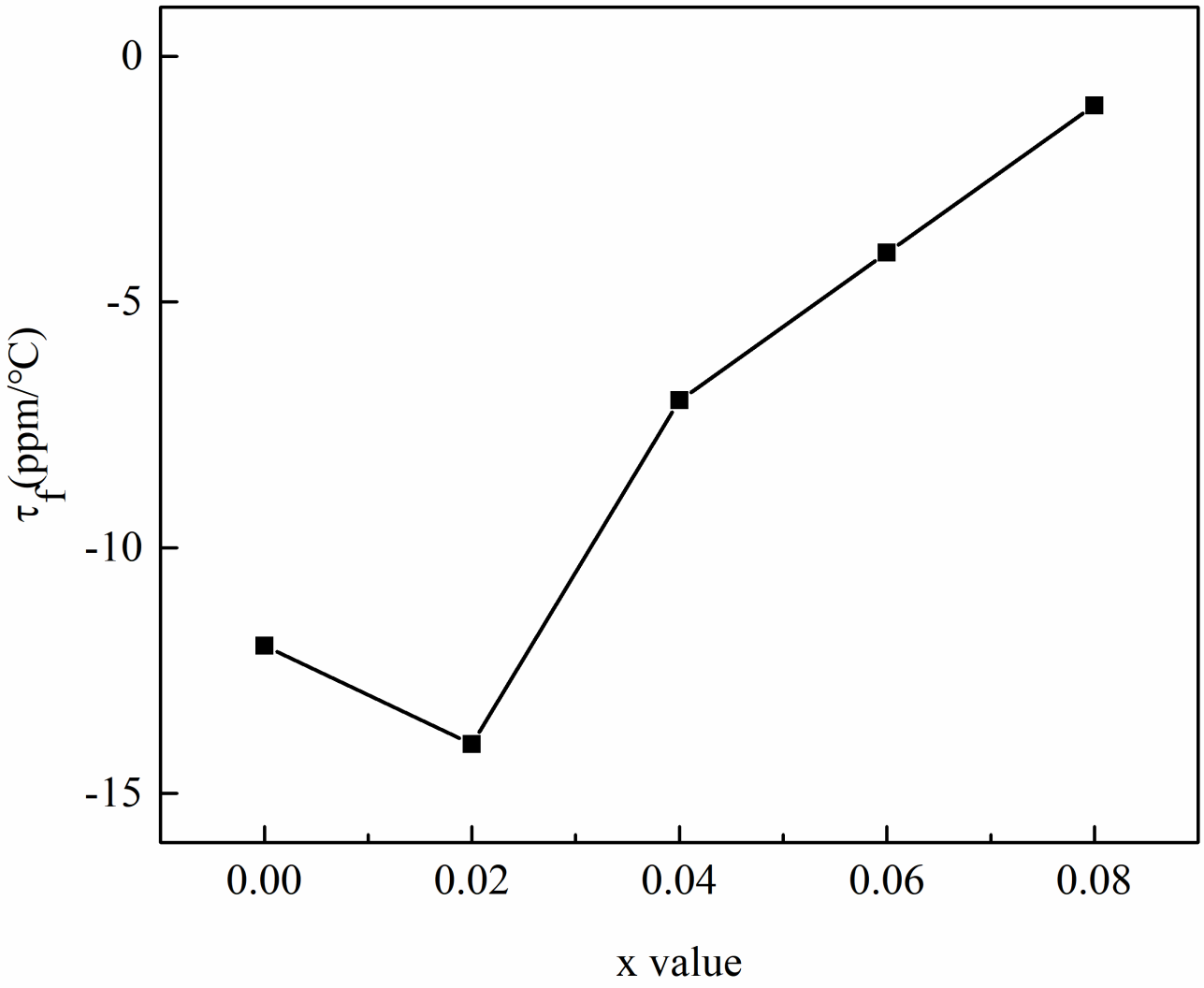

Figure 5

f values of the Li3(Mg1-xZnx)2SbO6 (0.00≤x≤0.08) ceramics sintered at 1325 °C.